









RESEARCH ARTICLE OPEN ACCESS

Application Research of Serum Fourier Transform Infrared Spectroscopy in Early Detection of Osteoporosis

Weihsang Yang^{1,2}  | Jiahao Xu¹  | Daojie Huang³  | Shuang Xia¹  | Liang Li¹  | Yuwei Zhu⁴  | Hongjian Ji⁵  | Fengchao Shi¹ 

¹Department of Orthopedics, Affiliated Hospital 6 of Nantong University, Yancheng Third People's Hospital, Yancheng, Jiangsu, China | ²Orthopedic Diagnosis and Treatment Center, Tongling People's Hospital, Tongling, Anhui, China | ³Department of Neurology, The First People's Hospital of Nantong, The Second Affiliated Hospital of Nantong University, Nantong, Jiangsu, China | ⁴Department of Orthopedics, Suzhou BOE Hospital, Suzhou, Jiangsu, China | ⁵School of Pharmacy, Jiangsu Medical College, Yancheng City Therapeutic Drug Precision Testing Engineering Center, Yancheng, Jiangsu, China

Correspondence: Hongjian Ji (hongjianji2006@163.com) | Fengchao Shi (shifengchao1980@126.com)

Received: 28 March 2025 | **Revised:** 14 December 2025 | **Accepted:** 4 February 2026

Academic Editor: Khalique Ahmed

Keywords: Fourier transform infrared spectroscopy | low bone density | osteoporosis | serum

ABSTRACT

This study aims to differentiate early between patients with osteoporosis (OP) and low bone density (LBD) using Fourier transform infrared (FTIR) spectroscopy combined with the partial least squares-support vector machine (PLS-SVM) algorithm. The study included 78 patients aged 50–90 years, categorized into three groups based on bone mineral density (BMD): normal (N group), LBD group, and OP group. FTIR spectra of serum samples were acquired using potassium bromide pellets of uniform thickness, and PLS-SVM was employed for dimensionality reduction and classification. The results demonstrated an accuracy of 95%, 85%, and 90% for the N, LBD, and OP groups, respectively, in the test set. Second-derivative spectral analysis revealed that the spectral intensities at the specific wavenumbers of 2925, 2860, 1651, 1610, 1523, 1505, 1481, 1421, 1399, 1361, and 1139 cm^{-1} were lower in OP and LBD patients compared to the normal group, indicating differences in lipids, proteins, and amino acids. This study offers a promising new, noninvasive, cost-effective, and sensitive alternative for the early diagnosis of OP.

1 | Introduction

Osteoporosis (OP), a systemic skeletal disease marked by diminished bone mass and the degradation of bone tissue microstructure, significantly elevates the risk of fractures [1, 2]. The World Health Organization (WHO) categorizes OP as a condition where bone mineral density (BMD) is 2.5 standard deviations or more below the mean in healthy adults [3]. Epidemiological studies reveal that among individuals over 50, one-third of women and one-fifth of men are affected by OP [1]. Notably, the most prevalent fractures linked to OP involve the spine, hip, and forearm, with spinal and hip fractures being particularly

worrisome due to their strong association with increased disability and mortality rates [4]. Alarming, approximately 20% of patients suffering from osteoporotic hip fractures succumb within 6 months [5]. Furthermore, the economic implications of OP-related fractures are substantial, with direct medical expenditures surpassing \$17 billion annually in the United States and over €37 billion in Europe. This does not account for the indirect costs associated with long-term care and diminished productivity, which impose considerable financial strain on individuals, families, and society [6, 7]. Numerous studies also suggest that, with the global aging population accelerating, the prevalence of OP is projected to double by 2050, exacerbating the

Weihsang Yang, Jiahao Xu, and Daojie Huang have contributed equally to this work.

This is an open access article under the terms of the [Creative Commons Attribution](https://creativecommons.org/licenses/by/4.0/) License, which permits use, distribution and reproduction in any medium, provided the original work is properly cited.

Copyright © 2026 Weihsang Yang et al. *Journal of Spectroscopy* published by John Wiley & Sons Ltd.

economic burden [8]. These findings underscore the significance of OP as a critical public health concern. Consequently, the development of efficacious early screening methodologies is imperative for mitigating disease progression, diminishing disability rates, enhancing patient outcomes, and alleviating socioeconomic pressures.

Current clinical diagnosis of OP predominantly relies on imaging modalities and biochemical marker assessments. Although dual-energy X-ray absorptiometry (DXA) remains the gold standard for OP diagnosis through lumbar spine and hip BMD measurements, its clinical utility is constrained by insufficient sensitivity for early-stage detection, inability to monitor dynamic bone microstructural changes, and inherent limitations including radiation exposure and elevated costs [9]. Quantitative computed tomography, while capable of three-dimensional trabecular structure reconstruction, exhibits radiation doses approximately tenfold higher than DXA, compounded by substantial expenses and limited accessibility [10]. Quantitative ultrasound presents a radiation-free alternative predominantly applied to calcaneal assessment, though measurement accuracy is compromised by multiple confounding factors encompassing soft tissue thickness, transducer pressure variations, bone morphology, and operator-dependent techniques. Biochemical markers such as β -CTX and PINP, despite their capacity to dynamically monitor bone turnover, demonstrate compromised diagnostic specificity and sensitivity due to circadian rhythm fluctuations and individual metabolic variability, with no direct correlation to BMD measurements [11, 12]. These diagnostic constraints significantly hinder large-scale OP screening initiatives, particularly manifesting as inadequate sensitivity in populations with initial bone mass reduction. Alarming, approximately 50% of patients receive a diagnosis only following their first fragility fracture, thereby missing critical intervention opportunities. This clinical predicament underscores the urgent demand for developing rapid, noninvasive, and sensitive detection technologies. In previous studies, we achieved accurate differentiation between OP and LBD patients using surface-enhanced Raman spectroscopy (SERS) [13]. However, SERS relies on complex nanomaterial fabrication, involving cumbersome procedures and high costs. Recent advancements in Fourier-transform infrared spectroscopy (FTIR), leveraging its nondestructive nature and molecular fingerprinting capabilities, coupled with simplified sample preparation, cost-effectiveness, and operational ease, demonstrate considerable potential for biomedical applications and offer novel perspectives for the early diagnosis of OP.

FTIR operates as a vibrational spectroscopy technique that detects molecular energy transitions through characteristic mid-infrared absorption ($4000\text{--}400\text{ cm}^{-1}$). This method enables label-free, high-throughput analysis of biochemical composition and macromolecular structural changes in proteins, lipids, nucleic acids, and polysaccharides within biological specimens [14]. In orthopedic applications, FTIR provides quantitative insights into mineral crystallinity, collagen cross-linking patterns, and mineralization indices through detection of bone-specific spectral signatures: hydroxyapatite (PO_4^{3-} vibration at $1040\text{--}960\text{ cm}^{-1}$), collagen (amide I band at 1650 cm^{-1}), and carbonate (CO_3^{2-} peak at 870 cm^{-1}), thereby elucidating molecular pathology in conditions like OP and osteomalacia [15, 16]. FTIR's capacity to detect subtle biochemical alterations through spectral variations has established its utility in early detection and differential diagnosis of orthopedic disorders. Chaber et al. demonstrated its

diagnostic power by distinguishing osteomyelitis from radiologically similar Ewing's sarcoma through biopsy tissue analysis [17]. Furthermore, FTIR-based biopsy evaluations have achieved 92% accuracy in predicting treatment responses for pediatric Ewing's sarcoma patients through molecular-level correlations between spectral profiles and clinical outcomes [18, 19]. However, tissue biopsy limitations—including invasiveness, infection risks, and stringent sample requirements (anatomical precision, tissue integrity)—hinder longitudinal monitoring and population screening. This has driven exploration of alternative biological matrices. Peripheral blood serum emerges as an attractive candidate due to its clinical accessibility and suitability for serial sampling. As a metabolic repository, serum contains bone turnover biomarkers (ionized calcium and osteocalcin) and diverse metabolites (lipoproteins, advanced glycation end products), whose infrared spectra may encode molecular fingerprints of bone metabolism. Notably, while blood FTIR analysis has demonstrated diagnostic utility in sarcopenia screening and autoimmune disorders (rheumatoid arthritis, psoriasis, and ankylosing spondylitis) [20–24], its application to OP detection via peripheral blood serum remains unexplored—representing a critical research gap in non-invasive bone health assessment.

This study proposes a novel approach for early-stage discrimination between osteopenia and OP through serum FTIR spectroscopy combined with partial least squares-support vector machine (PLS-SVM) analysis. To our knowledge, this investigation represents the first reported application of serum-based FTIR spectral analysis combined with machine learning algorithms for OP classification. We anticipate that this approach could establish a new diagnostic paradigm characterized by early detection capability, noninvasiveness, cost-effectiveness, and enhanced sensitivity for OP screening. The experimental workflow is illustrated in the Graphical Abstract.

2 | Materials and Methods

2.1 | Research Subjects

This study enrolled patients (50–90 years) undergoing BMD assessment at the Sixth People's Hospital Affiliated to Nantong University between January and October 2024. Exclusion criteria comprised: (1) concurrent metabolic disorders other than OP (diabetes mellitus, thyroid dysfunction, and malignancies); (2) secondary OP; (3) autoimmune-mediated bone diseases (rheumatoid arthritis, ankylosing spondylitis); (4) prolonged use (> 3 months) of bone-modifying medications (corticosteroids, thyroid hormones, thiazide diuretics, and antiretroviral agents); and (5) recent fragility fractures (≤ 6 months). Following WHO diagnostic criteria using DXA measurements of lumbar spine and hip BMD, participants were stratified into three cohorts: Normal (N-group, T-score ≥ -1.0), low bone density (LBD-group, $-2.5 < \text{T-score} < -1.0$), and OP (OP-group, T-score ≤ -2.5). The final cohort comprised 78 participants (N, $n = 24$; LBD, $n = 30$; OP, $n = 24$). This investigation was conducted in strict compliance with Declaration of Helsinki principles under ethical approval from the institutional review board (Sixth People's Hospital Affiliated to Nantong University), with all participants providing written informed consent.

2.2 | Sample Collection

Blood samples were collected from fasting participants in the morning by nursing staff from the same department following standard biochemical testing protocols. Subsequently, 5 mL of blood was preserved in anticoagulant tubes and allowed to stand at 4°C for temporary storage. Within 8 h postcollection, the samples were centrifuged at 4°C and 4000 rpm for 10 min. The resulting supernatant was then transferred into 500 μ L cryotubes, which were properly labeled according to their respective groups and ultimately stored in a -80°C freezer for subsequent spectroscopic analysis.

2.3 | FTIR Spectral Acquisition

Serum samples were subjected to passive thawing at ambient temperature (25°C) for 40 min prior to analysis. Aliquots (50 μ L) were deposited onto pre-cleaned glass slides and thermally desiccated under a calibrated heating lamp (38°C, 20 min). Spectral acquisition employed the potassium bromide (KBr) pellet technique: 150 mg of spectroscopic-grade KBr was homogenized with dehydrated serum residues in an agate mortar through mechanical trituration. The resultant mixture was compressed (20 MPa, 1 min) using an HY-12 hydraulic press to fabricate translucent pellets (0.5 mm thickness). Infrared spectra were recorded on a Shimadzu IRAffinity-1 spectrometer (the 400–4000 cm^{-1} region, 4 cm^{-1} resolution) with 32 co-added scans per measurement. Each specimen underwent triplicate analyses following background correction using pure KBr pellets. Spectral data analysis utilized triplicate-averaged measurements per specimen.

2.4 | Data Processing and Analysis

Clinical data analysis was performed using SPSS 27.0, with continuous variables expressed as mean \pm standard deviation ($\bar{x} \pm s$) and analyzed via one-way ANOVA. The normality of the data distribution for each group was confirmed using the Shapiro–Wilk test, and all groups demonstrated a normal distribution. Categorical variables were presented as frequency distributions with chi-square testing for intergroup comparisons. Two-tailed statistical significance was established at $p < 0.05$, with multivariable covariance analysis implemented for age and gender adjustments when required.

Spectral preprocessing was performed using Origin 2022. Baseline correction was first applied using the second derivative method to identify the anchor points for baseline alignment. Subsequently, the spectra were smoothed using the Savitzky–Golay method with a window width of 20 points and a polynomial order of 2. Following this, min-max normalization was applied to the spectral data. Group-specific averaged spectra (N, LBD, and OP) with standard deviations were computed. To enhance spectral resolution and minimize baseline distortions, second-derivative transformations were applied—a validated technique for resolving overlapping absorption bands in infrared spectroscopy, where absorption peaks manifest as distinct minima [25].

Machine learning implementation utilized scikit-learn 1.6 with 75:25 train-test split (58:20 samples). PLS, a supervised dimensionality reduction technique, constructs latent variables by maximizing covariance between independent (X) and dependent (Y) variable matrices. Particularly effective for high-dimensional datasets where predictors surpass sample size, PLS demonstrates

superior performance to Principal component analysis in spectral data processing [26, 27]. PLS dimensionality reduction incorporated 10-fold cross-validation optimized through mean squared error prediction (MSEP) and X-Y correlation coefficients. SVM operates by identifying an optimal hyperplane in high-dimensional space to maximize classification margins, thereby enhancing model generalizability while maintaining robustness to feature space dimensionality [28]. SVM training employed exhaustive grid search with leave-one-out cross-validation (LOOCV) for hyperparameter tuning, maintaining test set integrity for final validation. Model performance was quantified through sensitivity (true positive rate, equation (1)), specificity (true negative rate, equation (2)), and accuracy (overall classification rate and equation (3)), complemented by confusion matrices and ROC curves graphically demonstrating model efficacy.

$$\text{Sensitivity} = \frac{\text{TP}}{\text{TP} + \text{FN}} \quad (1)$$

$$\text{Specificity} = \frac{\text{TN}}{\text{TN} + \text{FP}} \quad (2)$$

$$\text{Accuracy} = \frac{\text{TP} + \text{TN}}{\text{TP} + \text{TN} + \text{FP} + \text{FN}} \quad (3)$$

3 | Results

3.1 | Demographic and Clinical Profiles

Table 1 summarizes demographic characteristics and clinical parameters across study cohorts. Statistical analysis revealed significant intergroup differences in gender distribution ($p = 0.037$), with female predominance demonstrating a progressive increase from 51.20% (N) to 87.50% (OP), though no significance existed between the N and LBD groups ($p = 0.496$). Age distribution exhibited a significant age gradient ($p < 0.001$), rising sequentially from 59.13 \pm 7.39 years (N) through 67.83 \pm 10.60 years (LBD) to 75.67 \pm 7.20 years (OP). Body mass index and hepatic/renal function markers (ALT, AST, BUN, and Cr) showed no statistical significance ($p > 0.05$). Multivariate covariance analysis confirmed group classification as the primary contributor to spectral variance ($p < 0.001$, partial $\eta^2 = 0.434$), substantially exceeding gender ($p = 0.028$, $\eta^2 = 0.308$) and age ($p = 0.089$, $\eta^2 = 0.263$) effects. These findings confirm that serum spectral alterations principally reflect bone metabolic pathology, independent of baseline demographic variations.

3.2 | Spectral Profiles and Band Assignments

Figure 1 depicts preprocessed average FTIR spectra of serum samples from N, LBD, and OP groups, with shaded regions denoting spectral standard deviations. The three cohorts exhibited comparable spectral patterns across the mid-infrared region (4000–400 cm^{-1}), suggesting conserved molecular constituents in the serum matrix. Table 2 summarizes the vibration band assignments based on established literature references [24, 29–43].

3.3 | Second Derivative Infrared Spectroscopy Analysis

Second-derivative transformation enhanced spectral resolution by amplifying subtle infrared absorption variations. As illustrated

TABLE 1 | Demographic and clinical data of the three patient groups^a.

Project	N (n = 24)	LBD (n = 30)	OP (n = 24)	F/ χ^2	p value
Sex, female	13 (51.20%) ^d	19 (63.30%) ^d	21 (87.50%)	6.599	0.037*
Age, year	59.13 ± 7.39 ^{c,d}	67.83 ± 10.60 ^{b,d}	75.67 ± 7.20 ^{b,c}	21.602	< 0.001*
BMI, kg/m ²	24.98 ± 2.88	24.65 ± 3.20	25.02 ± 5.06	0.081	0.922
Uric acid, μ mol/L	277.73 ± 95.69	293.04 ± 85.15	266.39 ± 69.73	0.681	0.509
Creatinine, μ mol/L	62.25 ± 11.02	70.97 ± 23.78	64.45 ± 19.99	1.494	0.231
ALT, U/L	27.24 ± 13.05	24.09 ± 17.36	19.88 ± 8.32	1.726	0.185
AST, U/L	28.45 ± 10.89	22.21 ± 10.27	25.44 ± 14.05	1.899	0.157

Note: Superscript letters denote statistically significant differences ($p < 0.05$). n, number of cases. ALT, alanine aminotransferase. AST, aspartate aminotransferase. The p value for the comparison marked with * ($p < 0.001$) is 3.8999E - 8.

Abbreviation: BMI, body mass index.

^aValues are expressed as mean ± standard deviation.

^bvs. Normal group (N).

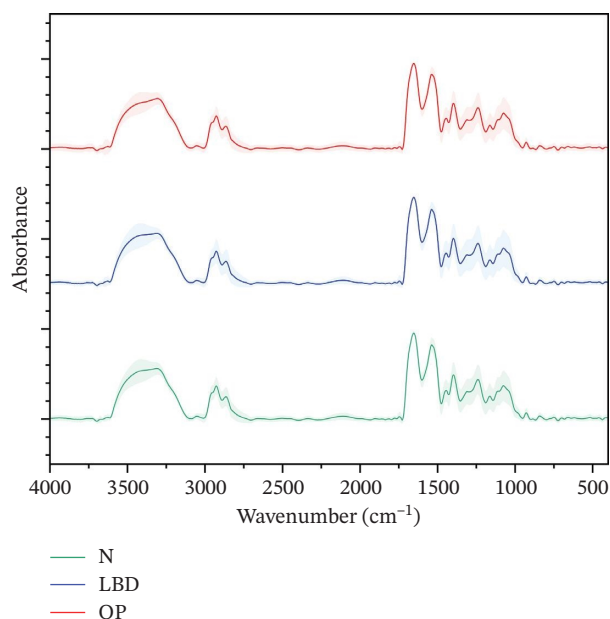
^cvs. Low bone density group (LBD).

^dvs. Osteoporosis group (OP).

in Figure 2, intergroup disparities predominantly clustered within 3000–2800 and 1700–900 cm^{-1} regions. Further details show that the band intensities in the serum of OP and LBD patients at 2925, 2860, 1651, 1610, 1523, 1505, 1481, 1421, 1399, 1361, and 1139 cm^{-1} are lower than those in the normal group (Supporting Figure 1). These spectral bands correspond to the stretching vibrations of C-H bonds in CH_2 , amide I, amide II, shear vibrations of C-H bonds in CH_2 , bending vibrations of CH_3 , and stretching vibrations of C-O bonds in threonine, tyrosine, and serine. These alterations collectively indicate perturbations in lipid profiles, protein conformations, and amino acid metabolism associated with bone metabolic disorders.

3.4 | PLS Component Optimization

PLS analysis was employed for spectral feature extraction and dimensionality reduction. Figure 3(a) demonstrates the MSEP decreasing sharply with initial component additions before plateauing at 13 components (MSEP = 0.0504). The first 13 latent

**FIGURE 1** | Average FTIR spectra of serum samples from three patient groups.

variables exhibited strong X-Y correlation ($r = 0.959$) and cumulative determination ($R^2 = 0.919$), explaining 91.9% of spectral variance. K-fold cross-validation confirmed component optimization, ensuring robust model generalizability. These dimensionality-reduced features were subsequently utilized in SVM modeling for OP screening.

3.5 | SVM Classification Performance

The dimensionality-reduced PLS components were subsequently fed into the SVM model using a 75:25 training-test split ratio. Parameter optimization was performed through grid search coupled with LOOCV, wherein each iteration reserved one sample for validation while training on the remaining specimens—a process repeated across all samples. This rigorous approach maximizes data utilization while mitigating overfitting risks inherent in small sample studies, yielding validation metrics that better represent true model generalizability [44].

Optimal model performance was achieved with a linear kernel function and penalty coefficient $C = 0.1$. Training set validation outcomes (Figure 4(a)) demonstrated 89.66% overall accuracy, with respective sensitivities of 88%, 86%, and 94% for N, LBD, and OP groups, accompanied by specificity values surpassing 90% across all categories. ROC analysis revealed exceptional discriminative capacity with AUC values of 0.958, 0.928, and 0.997 for the three groups (Figure 4(b)), indicating robust interclass differentiation (Table 3).

Independent test set evaluation (Table 4) confirmed model efficacy, particularly for OP group classification showing 90% accuracy, 100% sensitivity, and 87% specificity. The confusion matrix (Figure 5(a)) analysis identified three misclassifications among 20 test samples (1 N-group and 2 LBD-group instances). Corresponding AUC values of 0.945, 0.802, and 0.987 for N, LBD, and OP groups respectively underscored strong diagnostic performance, particularly for LBD and OP patient stratification (Figure 5(b)).

4 | Discussion

The pathogenesis of OP exhibits multifactorial etiology, with gender and age serving as predominant determinants [45, 46]. Accelerating global demographic aging has driven a progressive rise in OP prevalence, emerging as a critical public

TABLE 2 | FTIR spectral peak positions and assignments for serum samples.

Peak positions (cm ⁻¹)	Tentative assignments	References
3301	N-H stretching vibrations in proteins, O-H stretching vibrations in water	[24, 29]
3052	N-H stretching vibrations in proteins	[24, 29]
2958	Fatty acids, cholesterol, Aminoacid, Asymmetric C-H stretching in CH ₃	[30]
2927	Phospholipids, free fatty acids, Asymmetric C-H stretching in CH ₂	[31]
2863	Phospholipids, free fatty acids, Symmetric C-H stretching in CH ₂	[32]
1700–1600	Collagen, Amide I	[33]
1654	α -helices, β -turns or 3_{10} -helices in amide I	[34]
1500–1600	Amide II	[35]
1539	C-N stretching and C-N-H bending vibrations in amide II	[36]
1445	Scissoring bending of C-H in CH	[37]
1398	Aminoacid side, chains, fatty acids, Symmetric CH ₃ bending vibration	[38, 39]
1311	Coupling C-N stretching and N-H bending in amide III bands	[40]
1238	Amide III, Asymmetric P=O stretching in PO ₂ ⁻	[41]
1162	C-O stretching in serine, threonine, tyrosine	[42]
1073	Symmetric P=O stretching in PO ₂ ⁻	[43]

health challenge. While BMD assessment remains recommended for elderly screening, this methodology faces substantial implementation barriers due to prohibitive costs, radiation exposure concerns, and limited patient health literacy [47]. Recent advancements in FTIR spectroscopy have demonstrated considerable diagnostic potential across pathologies, providing novel approaches for early OP detection. Our investigation achieved successful discrimination of serum profiles among N, LBD, and OP cohorts through FTIR spectroscopy coupled with PLS-SVM algorithms, attaining test set classification accuracies of 95%, 85%, and 90%, respectively. These findings highlight the clinical viability of serum FTIR technology for OP diagnosis, demonstrating its capacity as a non-invasive, sensitive, specific, and cost-effective alternative for early screening implementation.

Serum FTIR spectroscopy measures molecular absorption of infrared radiation, generating characteristic spectra where peak positions correlate with vibrational modes of specific functional group bonds, thereby revealing sample biochemical composition [25]. Comparative analysis of second-derivative infrared spectra (Figure 2) across the three serum groups demonstrates distinct spectral deviations between OP/LBD patients and healthy controls at key wavelengths. In the 3000–2800 cm⁻¹ region, diminished C-H stretching vibrations at 2925 cm⁻¹ (CH₂ asymmetric) and 2860 cm⁻¹ (CH₂ symmetric) suggest structural alterations in lipid chain organization. This phenomenon could be attributed to two primary factors: (1) enhanced lipid peroxidation in bone metabolism disorders potentially disrupts spatial arrangement of CH₂ groups within membrane phospholipid bilayers and (2) reduced low-density lipoprotein and free fatty acid concentrations may attenuate vibrational signals from long-chain alkanes. These observations align with documented evidence of marrow fat accumulation and dyslipidemia in OP pathogenesis [48, 49]. Notably, clinical studies identify hyperlipidemia as a shared

risk factor for OP and atherosclerosis [50, 51], where lipid oxidation products activate PPAR γ receptors, subsequently impairing Wnt signaling and age-related bone formation [52]. Such mechanisms substantiate lipid homeostasis disruption as a potential synergistic contributor to BMD loss. In the 1700–1600 cm⁻¹ region, attenuated amide I (1651 cm⁻¹, C=O stretch) and amide II (1523–1505 cm⁻¹, C-N stretch/N-H bend) bands indicate protein conformational changes. The amide I reduction may reflect decreased α -helix content in serum albumin or bone-related proteins (e.g., osteocalcin and collagen I), while amide II alterations suggest β -sheet structural perturbations. Particularly, impaired collagen metabolism in OP patients could reduce hydroxyproline crosslinking [53], potentially modifying interprotein hydrogen bonding networks that influence amide vibration characteristics. Spectral variations at 1399 cm⁻¹ (CH₃ deformation) and 1139 cm⁻¹ (C-O stretch) within 1400–1000 cm⁻¹ reveal amino acid metabolic abnormalities. The attenuated C-O vibrations (1139 cm⁻¹) imply oxidative modifications in hydroxyl amino acids (threonine, tyrosine, serine) side chains. Crucially, tyrosine phosphorylation—a key regulator of osteoblast differentiation—may be compromised, potentially suppressing bone formation via Wnt/ β -catenin pathway inhibition [54, 55]. Concurrent reductions in CH₂ scissoring (1421 cm⁻¹) and CH₃ bending (1361 cm⁻¹) vibrations further support lipid acyl chain oxidative cleavage, a process potentially exacerbating osteoclast activity through NF- κ B pathway activation [56, 57]. Collectively, these serum compositional and structural alterations create discernible spectral signatures, establishing a foundation for multivariate statistical discrimination of pathological states.

In this study, PLS was applied to second-derivative spectral data, with K-fold cross-validation incorporating both X/Y explained variance and prediction mean squared error to optimize latent variable selection. These refined components were subsequently

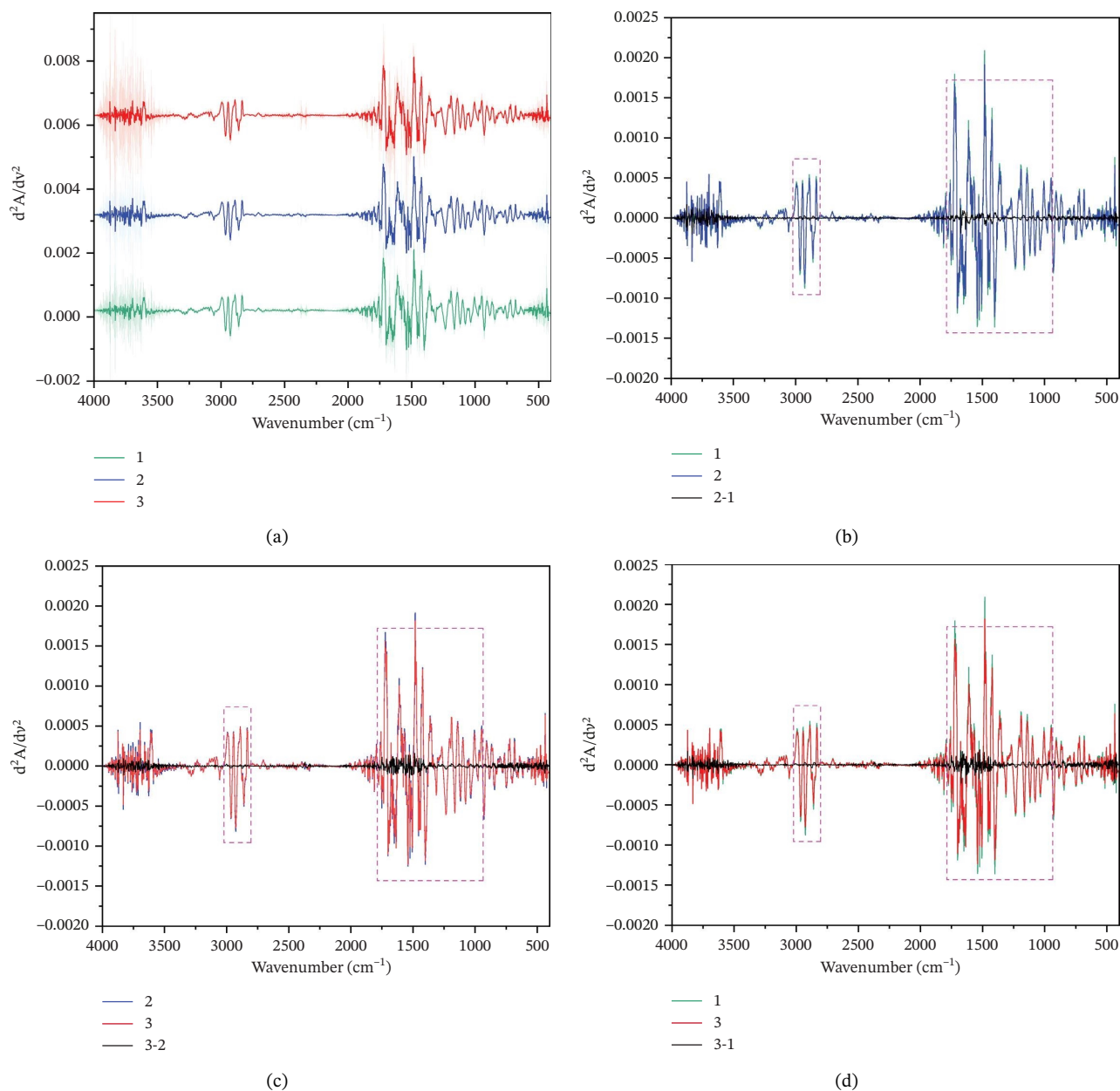


FIGURE 2 | (a) Second derivatives of serum FTIR spectra from the normal group (1), low bone density group (2), and osteoporosis group (3), along with difference spectra (b–d) between the mean derivatives of respective group pairs.

fed into an SVM classifier, where LOOCV fine-tuned model parameters on training data prior to test set validation. The confusion matrix (Figure 5(a)) revealed test set sensitivities of 86%, 75%, and 100% across patient groups, while ROC (Figure 5(b)) analysis demonstrated excellent classification accuracy (AUCs: 0.945, 0.802, and 0.987). These metrics collectively confirm the PLS-SVM framework's reliability and efficacy for OP spectral data analysis.

This study acknowledges several limitations requiring consideration. First, the restricted sample size may constrain the generalizability of findings. Second, despite employing multivariate analysis of covariance to address demographic

disparities, inherent age and gender distribution differences among study cohorts could persist as confounding factors influencing spectral signatures, potentially compromising model accuracy and specificity. Future investigations should prioritize balanced demographic sampling to mitigate such biases. Furthermore, the exclusive focus on serum biomarkers neglects complementary clinical indicators; integrating multimodal data streams could improve diagnostic performance through comprehensive metabolic profiling. While the PLS-SVM algorithm demonstrated robust training-test set concordance, its translational utility necessitates validation in real-world clinical environments. Prospective cohort studies are warranted to assess practical applicability, ultimately

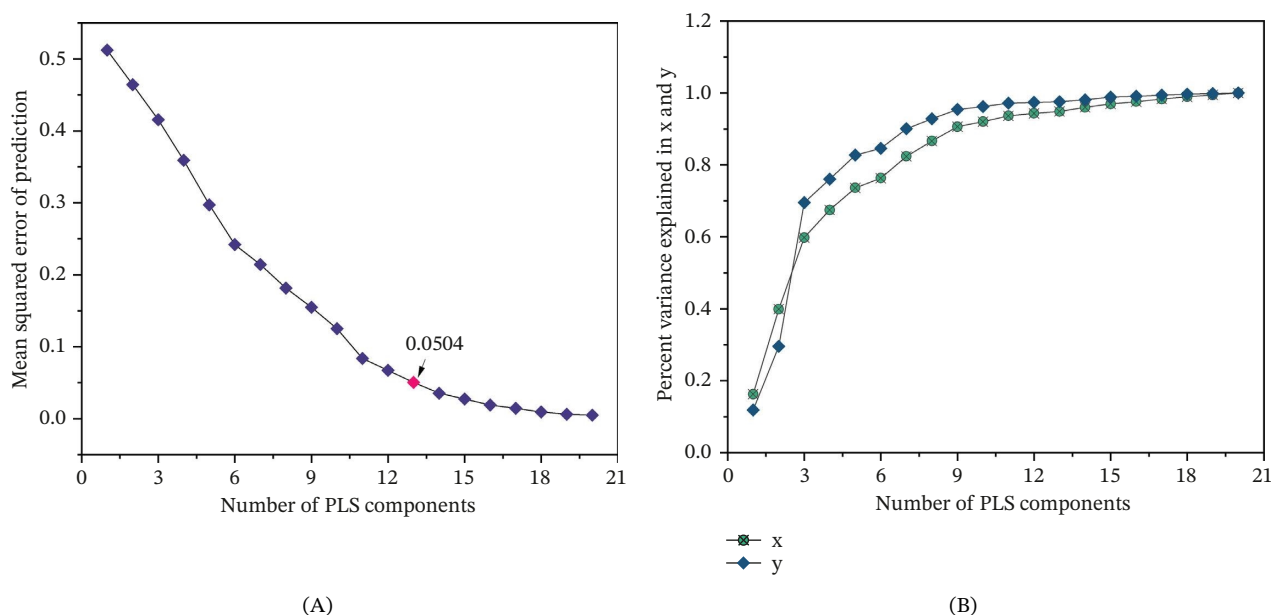


FIGURE 3 | (A) Mean squared error of prediction generated using the first 20 PLS components and (B) cumulative percentage variance of X (predictor variables) and Y (response variables) explained by the components.

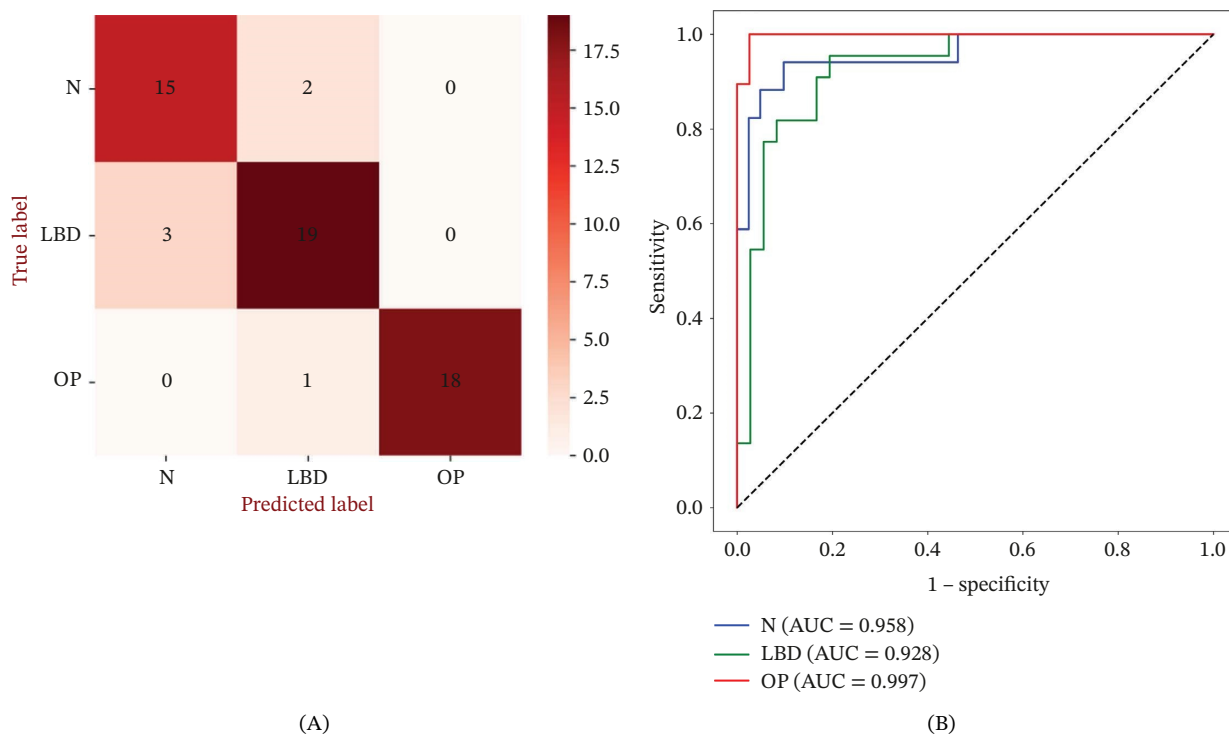


FIGURE 4 | (A) Confusion matrix and (B) ROC curve of the PLS-SVM model in the training set.

TABLE 3 | Performance evaluation of the PLS-SVM model on the training set.

Groups	Accuracy (%)	Sensitivity (%)	Specificity (%)
N	91	88	93
LBD	87	86	92
OP	98	94	100

TABLE 4 | Performance evaluation of the PLS-SVM model on the test set.

Groups	Accuracy (%)	Sensitivity (%)	Specificity (%)
N	95	86	100
LBD	85	75	92
OP	90	100	87

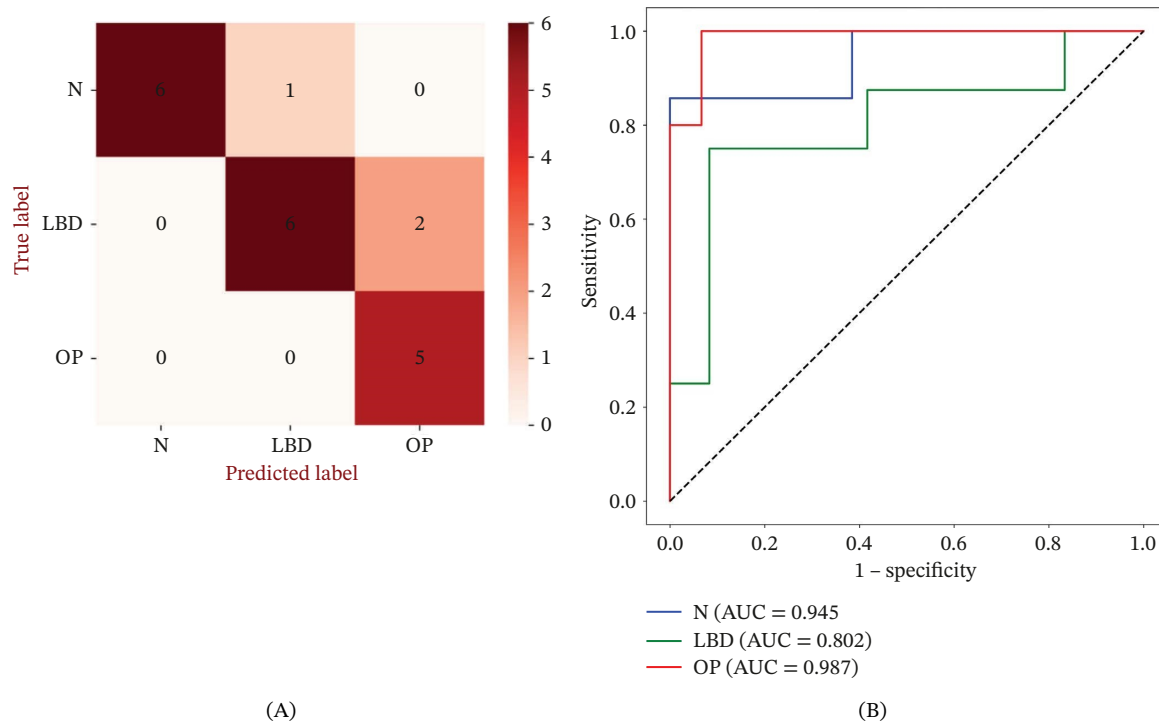


FIGURE 5 | (A) Confusion matrix and (B) ROC curve of the PLS-SVM model in the test set.

advancing OP diagnostic protocols for early intervention strategies.

5 | Conclusion

This study first utilized serum FTIR combined with the PLS-SVM method to make early differentiation between OP and LBD patients, with accuracy rates of 95%, 85%, and 90% in the test set. The research found that the peak intensity of serum spectra at certain wavelengths in OP and LBD patients was lower than in the normal group, reflecting biochemical changes in lipids, proteins, and amino acids, which are closely linked to issues with bone metabolism. The PLS-SVM method performed exceptionally in handling high-dimensional spectral data, effectively enhancing the classification performance of the model. This study offers a noninvasive, cost-effective, and sensitive way to screen for OP early on. Future research should further expand the sample size, balance the age and gender mix, and incorporate multimodal data for a thorough assessment to improve the usability and reliability of the model. Prospective cohort studies should validate the model's performance in real clinical settings, which is expected to provide better support for early diagnosis and intervention of OP.

Author Contributions

Weihang Yang conducted the experiments, analyzed the data, and drafted the manuscript. Jiahao Xu collaborated in the experimental procedures and participated in sample collection. Daojie Huang was responsible for collecting and organizing the clinical data. Shuang Xia, Liang Li, and Yuwei Zhu contributed to sample collection and provided interpretations of the results. Hongjian Ji conceived the study concept and critically revised the manuscript. Fengchao Shi supervised the study and provided funding.

Funding

This work was supported by the Yancheng Science and Technology Bureau (YCBE202423, YCBE202442), the Yancheng Health Commission (YK2024157), and the Nantong University Clinical Basic Research Special Fund (2023JZ027).

Disclosure

All authors reviewed and approved the final version of the manuscript.

Ethics Statement

This study was approved by the Ethics Review Committee of Affiliated Hospital 6 of Nantong University (2021-068-01). All participants provided written informed consent prior to their involvement in the study.

Conflicts of Interest

The authors declare no conflicts of interest.

Data Availability Statement

The datasets used and/or analyzed during the current study are available from the corresponding authors upon reasonable request. Requests can be directed to the corresponding author's email at hongjian.ji2006@163.com.

References

1. E. Rentzeperi, S. Pegiou, I. Tsakiridis, et al., "Diagnosis and Management of Osteoporosis: A Comprehensive Review of Guidelines," *Obstetrical and Gynecological Survey* 78, no. 11 (2023): 657–681, <https://doi.org/10.1097/OGX.0000000000001181>.
2. C. Ayers, D. Kansagara, B. Lazur, R. Fu, A. Kwon, and C. Harrod, "Effectiveness and Safety of Treatments to Prevent Fractures in People With Low Bone Mass or Primary Osteoporosis: A Living Systematic Review and Network Meta-Analysis for the American College of Physicians," *Annals of Internal Medicine* 176, no. 2 (2023): 182–195, <https://doi.org/10.7326/M22-0684>.

3. P. L. Xiao, A. Y. Cui, C. J. Hsu, et al., "Global, Regional Prevalence, and Risk Factors of Osteoporosis According to the World Health Organization Diagnostic Criteria: A Systematic Review and Meta-Analysis," *Osteoporosis International* 33, no. 10 (2022): 2137–2153, <https://doi.org/10.1007/s00198-022-06454-3>.
4. S. M. Tarrant and Z. J. Balogh, "The Global Burden of Surgical Management of Osteoporotic Fractures," *World Journal of Surgery* 44, no. 4 (2020): 1009–1019, <https://doi.org/10.1007/s00268-019-05237-y>.
5. Y.-Y. Zhang, N. Xie, X.-D. Sun, et al., "Insights and Implications of Sexual Dimorphism in Osteoporosis," *Bone Research* 12, no. 1 (2024): 8, <https://doi.org/10.1038/s41413-023-00306-4>.
6. E. Boucher, B. Rosgen, and E. Lang, "Efficacy of Calcitonin for Treating Acute Pain Associated With Osteoporotic Vertebral Compression Fracture: An Updated Systematic Review," *Canadian Journal of Emergency Medicine* 22, no. 3 (2020): 359–367, <https://doi.org/10.1017/cem.2019.490>.
7. Y. Shen, X. Huang, J. Wu, et al., "The Global Burden of Osteoporosis, Low Bone Mass, and Its Related Fracture in 204 Countries and Territories, 1990–2019," *Frontiers in Endocrinology* 13 (2022): 882241, <https://doi.org/10.3389/fendo.2022.882241>.
8. C.-W. Sing, T.-C. Lin, S. Bartholomew, et al., "Global Epidemiology of Hip Fractures: Secular Trends in Incidence Rate, Post-Fracture Treatment, and All-Cause Mortality," *Journal of Bone and Mineral Research* 38, no. 8 (2023): 1064–1075, <https://doi.org/10.1002/jbmr.4821>.
9. Y. Liu, X.-H. Meng, C. Wu, et al., "Variability in Performance of Genetic-Enhanced Dxa-Bmd Prediction Models Across Diverse Ethnic and Geographic Populations: A Risk Prediction Study," *PLoS Medicine* 21, no. 8 (2024): e1004451, <https://doi.org/10.1371/journal.pmed.1004451>.
10. E. M. Lewiecki, "Imaging Technologies for Assessment of Skeletal Health in Men," *Current Osteoporosis Reports* 11, no. 1 (2013): 1–10, <https://doi.org/10.1007/s11914-012-0128-x>.
11. C. M. Swanson, S. A. Shea, W. M. Kohrt, et al., "Sleep Restriction With Circadian Disruption Negatively Alter Bone Turnover Markers in Women," *The Journal of Clinical Endocrinology and Metabolism* 105, no. 7 (2020): 2456–2463, <https://doi.org/10.1210/clinem/dgaa232>.
12. B. Luo, X. Zhou, Q. Tang, Y. Yin, G. Feng, and L. Chen, "Circadian Rhythms Affect Bone Reconstruction by Regulating Bone Energy Metabolism," *Journal of Translational Medicine* 19, no. 1 (2021): 410, <https://doi.org/10.1186/s12967-021-03068-x>.
13. W. Yang, S. Xia, X. Jia, et al., "Utilizing Surface-Enhanced Raman Spectroscopy for the Adjunctive Diagnosis of Osteoporosis," *European Journal of Medical Research* 29, no. 1 (2024): 476, <https://doi.org/10.1186/s40001-024-02081-2>.
14. P. Koziol, D. Liberda, W. M. Kwiatek, and T. P. Wrobel, "Macromolecular Orientation in Biological Tissues Using a Four-Polarization Method in Ft-Ir Imaging," *Analytical Chemistry* 92, no. 19 (2020): 13313–13318, <https://doi.org/10.1021/acs.analchem.0c02591>.
15. M. Pedrosa, M. T. Ferreira, L. A. E. Batista de Carvalho, M. P. M. Marques, and F. Curate, "The Association of Osteochemometrics and Bone Mineral Density in Humans," *American Journal of Physical Anthropology* 176, no. 3 (2021): 434–444, <https://doi.org/10.1002/ajpa.24283>.
16. J. J. Miszkiewicz, F. Valentin, C. Vrahnas, et al., "Bone Loss Markers in the Earliest Pacific Islanders," *Scientific Reports* 11, no. 1 (2021): 3981, <https://doi.org/10.1038/s41598-021-83264-3>.
17. R. Chaber, C. J. Arthur, J. Depciuch, et al., "Distinguishing Ewing Sarcoma and Osteomyelitis Using Ftir Spectroscopy," *Scientific Reports* 8, no. 1 (2018): 15081, <https://doi.org/10.1038/s41598-018-33470-3>.
18. R. Chaber, C. J. Arthur, K. Łach, et al., "Predicting Ewing Sarcoma Treatment Outcome Using Infrared Spectroscopy and Machine Learning," *Molecules* 24, no. 6 (2019): 1075, <https://doi.org/10.3390/molecules24061075>.
19. R. Chaber, K. Łach, C. J. Arthur, et al., "Prediction of Ewing Sarcoma Treatment Outcome Using Attenuated Tissue Reflection Ftir Tissue Spectroscopy," *Scientific Reports* 8, no. 1 (2018): 12299, <https://doi.org/10.1038/s41598-018-29795-8>.
20. R. V. d M. Freitas, D. L. D. de Freitas, I. R. D. de Oliveira, et al., "Fourier-Transform Infrared Spectroscopy as a Screening Tool for Osteosarcopenia in Community-Dwelling Older Women," *The Journals of Gerontology, Series A: Biological Sciences and Medical Sciences* 78, no. 9 (2023): 1543–1549, <https://doi.org/10.1093/gerona/glad081>.
21. I. Kokot, S. Mazurek, A. Piwowar, et al., "Comparative Profiling of Serum Biomarkers and Atr-Ftir Spectroscopy for Differential Diagnosis of Patients With Rheumatoid and Psoriatic Arthritis—a Pilot Study," *Spectrochimica Acta Part A: Molecular and Biomolecular Spectroscopy* 321 (2024): 124654, <https://doi.org/10.1016/j.saa.2024.124654>.
22. K. Durluk-Popińska, P. Żarnowiec, I. Konieczna-Kwinkowska, Ł. Lechowicz, J. Gawęda, and W. Kaca, "Correlations Between Auto-antibodies and the Atr-Ftir Spectra of Sera From Rheumatoid Arthritis Patients," *Scientific Reports* 11, no. 1 (2021): 17886, <https://doi.org/10.1038/s41598-021-96848-w>.
23. W. Shuai, X. Wu, C. Chen, et al., "Rapid Diagnosis of Rheumatoid Arthritis and Ankylosing Spondylitis Based on Fourier Transform Infrared Spectroscopy and Deep Learning," *Photodiagnosis and Photodynamic Therapy* 45 (2024): 103885, <https://doi.org/10.1016/j.pdpdt.2023.103885>.
24. X. Wu, W. Shuai, C. Chen, et al., "Rapid Screening for Autoimmune Diseases Using Fourier Transform Infrared Spectroscopy and Deep Learning Algorithms," *Frontiers in Immunology* 14 (2023): 1328228, <https://doi.org/10.3389/fimmu.2023.1328228>.
25. V. E. Sitnikova, M. A. Kotkova, T. N. Nosenko, T. N. Kotkova, D. M. Martynova, and M. V. Uspenskaya, "Breast Cancer Detection by Atr-Ftir Spectroscopy of Blood Serum and Multivariate Data-Analysis," *Talanta* 214 (2020): 120857, <https://doi.org/10.1016/j.talanta.2020.120857>.
26. Y. Yu, W. Chen, L. Wang, et al., "An Auxiliary Diagnostic Technology and Clinical Efficacy Evaluation in Knee Osteoarthritis Based on Serum Surface-Enhanced Raman Spectroscopy," *Spectrochimica Acta Part A: Molecular and Biomolecular Spectroscopy* 296 (2023): 122654, <https://doi.org/10.1016/j.saa.2023.122654>.
27. T. Shi, M. Zhu, Y. Chen, et al., "1h Nmr Combined With Chemometrics for the Rapid Detection of Adulteration in Camellia Oils," *Food Chemistry* 242 (2018): 308–315, <https://doi.org/10.1016/j.foodchem.2017.09.061>.
28. M.-P. Hosseini, A. Hosseini, and K. Ahi, "A Review on Machine Learning for Eeg Signal Processing in Bioengineering," *IEEE Reviews in Biomedical Engineering* 14 (2021): 204–218, <https://doi.org/10.1109/RBME.2020.2969915>.
29. C. Jin, A. Patel, J. Peters, S. Hodawadekar, and R. Kalyanaraman, "Quantum Cascade Laser Based Infrared Spectroscopy: A New Paradigm for Protein Secondary Structure Measurement," *Pharmaceutical Research* 40, no. 6 (2023): 1507–1517, <https://doi.org/10.1007/s11095-022-03422-8>.
30. P. Prada, B. Brunel, D. Moulin, et al., "Identification of Circulating Biomarkers of Crohn's disease and Spondyloarthritis Using Fourier Transform Infrared Spectroscopy," *Journal of Biophotonics* 16, no. 2 (2023): e202200200, <https://doi.org/10.1002/jbio.202200200>.
31. G. I. Dovbeshko, N. Y. Gridina, E. B. Kruglova, et al., "Ftir Spectroscopy Studies of Nucleic Acid Damage," *Talanta* 53, no. 1 (2000): 233–246, [https://doi.org/10.1016/s0039-9140\(00\)00462-8](https://doi.org/10.1016/s0039-9140(00)00462-8).
32. Z. Guleken, B. Ünübol, R. Bilici, et al., "Investigation of the Discrimination and Characterization of Blood Serum Structure in Patients With Opioid Use Disorder Using Ir Spectroscopy and Pca-Lda Analysis,"

- Journal of Pharmacy Biomedicine Analytical* 190 (2020): 113553, <https://doi.org/10.1016/j.jpba.2020.113553>.
33. Y.-C. Lee, C.-C. Chiang, P.-Y. Huang, et al., "Evidence of Preserved Collagen in an Early Jurassic Sauropodomorph Dinosaur Revealed by Synchrotron Ftir Microspectroscopy," *Nature Communications* 8, no. 1 (2017): 14220, <https://doi.org/10.1038/ncomms14220>.
 34. V. Virtanen, V. Tafintseva, R. Shaikh, et al., "Infrared Spectroscopy is Suitable for Objective Assessment of Articular Cartilage Health," *Osteoarthritis and Cartilage Open* 4, no. 2 (2022): 100250, <https://doi.org/10.1016/j.ocarto.2022.100250>.
 35. D. Sheng, Y. Wu, X. Wang, D. Huang, X. Chen, and X. Liu, "Comparison of Serum From Gastric Cancer Patients and From Healthy Persons Using Ftir Spectroscopy," *Spectrochimica Acta Part A: Molecular and Biomolecular Spectroscopy* 116 (2013): 365–369, <https://doi.org/10.1016/j.saa.2013.07.055>.
 36. F. Chen, C. Meng, H. Qu, et al., "Human Serum Mid-Infrared Spectroscopy Combined With Machine Learning Algorithms for Rapid Detection of Gliomas," *Photodiagnosis and Photodynamic Therapy* 35 (2021): 102308, <https://doi.org/10.1016/j.pdpdt.2021.102308>.
 37. A. Menikh, P. G. Nyholm, and J. M. Boggs, "Characterization of the Interaction of Ca²⁺ With Hydroxy and Non-Hydroxy Fatty Acid Species of Cerebroside Sulfate by Fourier Transform Infrared Spectroscopy and Molecular Modeling," *Biochemistry* 36, no. 12 (1997): 3438–3447, <https://doi.org/10.1021/bi961869q>.
 38. G. Cakmak, I. Togan, C. Uğuz, and F. Severcan, "Ft-Ir Spectroscopic Analysis of Rainbow Trout Liver Exposed to Nonylphenol," *Applied Spectroscopy* 57, no. 7 (2003): 835–841, <https://doi.org/10.1366/000370203322102933>.
 39. S. Garip, F. Bozoglu, and F. Severcan, "Differentiation of Mesophilic and Thermophilic Bacteria With Fourier Transform Infrared Spectroscopy," *Applied Spectroscopy* 61, no. 2 (2007): 186–192, <https://doi.org/10.1366/000370207779947486>.
 40. M. H. R. Mesquita-Britto, M. C. P. Mendonça, E. S. Soares, K. K. Sakane, and M. A. da Cruz-Höfling, "Inhibition of Vegf-Flk-1 Binding Induced Profound Biochemical Alteration in the Hippocampus of a Rat Model of Bbb Breakdown by Spider Venom. A Preliminary Assessment Using Ft-Ir Spectroscopy," *Neurochemistry International* 120 (2018): 64–74, <https://doi.org/10.1016/j.neuint.2018.07.011>.
 41. X. Yang, Q. Ou, W. Yang, Y. Shi, and G. Liu, "Diagnosis of Liver Cancer by Ftir Spectra of Serum," *Spectrochimica Acta Part A: Molecular and Biomolecular Spectroscopy* 263 (2021): 120181, <https://doi.org/10.1016/j.saa.2021.120181>.
 42. D. Sheng, X. Liu, W. Li, Y. Wang, X. Chen, and X. Wang, "Distinction of Leukemia Patients' and Healthy Persons' Serum Using Ftir Spectroscopy," *Spectrochimica Acta Part A: Molecular and Biomolecular Spectroscopy* 101 (2013): 228–232, <https://doi.org/10.1016/j.saa.2012.09.072>.
 43. C. Junhom, N. Weerapreeyakul, W. Tanthanuch, and K. Thumanu, "Partial Least Squares Regression and Fourier Transform Infrared (Ftir) Microspectroscopy for Prediction of Resistance in Hepatocellular Carcinoma Hepg2 Cells," *Experimental Cell Research* 351, no. 1 (2017): 82–90, <https://doi.org/10.1016/j.yexcr.2016.12.027>.
 44. N. Koutsouleris, D. B. Dwyer, F. Degenhardt, et al., "Multimodal Machine Learning Workflows for Prediction of Psychosis in Patients With Clinical High-Risk Syndromes and Recent-Onset Depression," *JAMA Psychiatry* 78, no. 2 (2021): 195–209, <https://doi.org/10.1001/jamapsychiatry.2020.3604>.
 45. W. Cai, J. Zhao, Y. Chen, et al., "Sting Regulates Aging-Related Osteoporosis by Mediating the Hk2-Vdac1 Mitochondrial Axis," *Free Radical Biology and Medicine* 225 (2024): 1–14, <https://doi.org/10.1016/j.freeradbiomed.2024.09.031>.
 46. L. Wang, W. Yu, X. Yin, et al., "Prevalence of Osteoporosis and Fracture in China: The China Osteoporosis Prevalence Study," *JAMA Network Open* 4, no. 8 (2021): e2121106, <https://doi.org/10.1001/jamanetworkopen.2021.21106>.
 47. K. E. Ensrud and C. J. Crandall, "Osteoporosis," *Annals of Internal Medicine* 167, no. 3 (2017): ITC17–ITC32, <https://doi.org/10.7326/AITC201708010>.
 48. C.-J. Li, Y. Xiao, Y.-C. Sun, et al., "Senescent Immune Cells Release Grancalcin to Promote Skeletal Aging," *Cell Metabolism* 33, no. 10 (2021): 1957–1973, <https://doi.org/10.1016/j.cmet.2021.08.009>.
 49. E. Galliera, M. G. Marazzi, C. Gazzaruso, et al., "Evaluation of Circulating Srage in Osteoporosis According to Bmi, Adipokines and Fracture Risk: A Pilot Observational Study," *Immunity and Ageing: Irish America* 14, no. 1 (2017): 13, <https://doi.org/10.1186/s12979-017-0097-0>.
 50. F. Parhami, A. Garfinkel, and L. L. Demer, "Role of Lipids in Osteoporosis," *Arteriosclerosis, Thrombosis, and Vascular Biology* 20, no. 11 (2000): 2346–2348, <https://doi.org/10.1161/01.atv.20.11.2346>.
 51. Y. Duan, K. Gong, S. Xu, F. Zhang, X. Meng, and J. Han, "Regulation of Cholesterol Homeostasis in Health and Diseases: From Mechanisms to Targeted Therapeutics," *Signal Transduction and Targeted Therapy* 7, no. 1 (2022): 265, <https://doi.org/10.1038/s41392-022-01125-5>.
 52. S. C. Manolagas, "From Estrogen-Centric to Aging and Oxidative Stress: A Revised Perspective of the Pathogenesis of Osteoporosis," *Endocrine Reviews* 31, no. 3 (2010): 266–300, <https://doi.org/10.1210/er.2009-0024>.
 53. E. Karna, L. Szoka, T. Y. L. Huynh, and J. A. Palka, "Proline-Dependent Regulation of Collagen Metabolism," *Cellular and Molecular Life Sciences: CMLS* 77, no. 10 (2020): 1911–1918, <https://doi.org/10.1007/s00018-019-03363-3>.
 54. G. Xi, X. Shen, C. J. Rosen, and D. R. Clemmons, "Irs-1 Functions as a Molecular Scaffold to Coordinate Igf-I/Igfbp-2 Signaling During Osteoblast Differentiation," *Journal of Bone and Mineral Research* 31, no. 6 (2016): 1300–1314, <https://doi.org/10.1002/jbmr.2791>.
 55. V. Deshmukh, A. L. O'Green, C. Bossard, et al., "Modulation of the Wnt Pathway Through Inhibition of Clk2 and Dyrk1a by Lorecivint as a Novel, Potentially Disease-Modifying Approach for Knee Osteoarthritis Treatment," *Osteoarthritis and Cartilage* 27, no. 9 (2019): 1347–1360, <https://doi.org/10.1016/j.joca.2019.05.006>.
 56. M. Abshirini, B. L. Ilesanmi-Oyelere, and M. C. Kruger, "Potential Modulatory Mechanisms of Action by Long-Chain Polyunsaturated Fatty Acids on Bone Cell and Chondrocyte Metabolism," *Progress in Lipid Research* 83 (2021): 101113, <https://doi.org/10.1016/j.plipres.2021.101113>.
 57. L. S. Graham, Y. Tintut, F. Parhami, et al., "Bone Density and Hyperlipidemia: The T-Lymphocyte Connection," *Journal of Bone and Mineral Research* 25, no. 11 (2010): 2460–2469, <https://doi.org/10.1002/jbmr.148>.

Supporting Information

Additional supporting information can be found online in the Supporting Information section. (*Supporting Information*)

Supporting Figure 1. (A–C) Mean second derivative difference spectra resulting from pairwise comparisons between the normal group (1), low bone density group (2), and osteoporosis group (3) in the region of 3000–2800 cm^{−1}; (D–F) corresponding spectra in the region of 1700–900 cm^{−1}.